This is an open access article published under an ACS AuthorChoice License, which permits copying and redistribution of the article or any adaptations for non-commercial purposes.

THE JOURNAL OF PHYSICAL CHEMISTRY B

Article

pubs.acs.org/JPCB

Interaction Mechanism Insights on the Solvation of Fullerene B_{80} with Choline-based Ionic Liquids

Gregorio García,[†] Mert Atilhan,*[,‡] and Santiago Aparicio*[,†]

[†]Department of Chemistry, University of Burgos, 09001 Burgos, Spain

[‡]Department of Chemical Engineering, Qatar University, P.O. Box 2713, Doha, Qatar

Supporting Information

ABSTRACT: Beyond carbon allotropes, other nanostructures such as fullerene B_{80} are attracting a growing interest due to their potential applications. The use of new materials based on fullerene B_{80} is still in a premature stage; however many of these applications would require the use of B_{80} in solution. This paper reports an unprecedented density functional theory (DFT) analysis on the interaction mechanism between B_{80} and two choline-based ionic liquids as a first insight for the fullerene B_{80} solvation by ionic liquids. The analysis of properties such as binding energies, charge distributions or intermolecular interactions shed light on the main features, which should govern interaction between ionic liquids and fullerene B_{80}. In addition, the optimization of systems composed by six ionic pairs around a fullerene B_{80} has supplied some information about the first solvation shell at the molecular level. As a summary, this paper provides the first insights in the rational design of ionic liquids with suitable properties for the solvation of B_{80}.

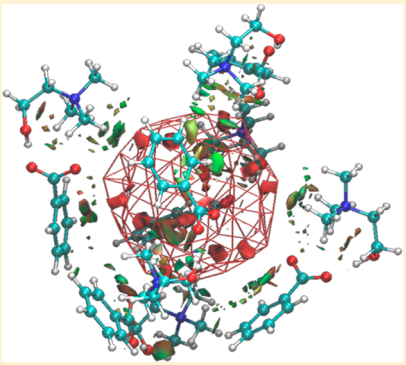

1. INTRODUCTION

There has been a growing interest in carbon nanostructures, such as fullerenes, nanotubes, and graphene flakes or sheets due to their promising potential as building blocks in a wide range of applications, such as biotechnology, nanobiomedicine, energy storage, and electronic devices.[1−7] Because of their significant promising structural, electronic, and chemical properties, there is also a rising attention in the search for other alternative nanostructures that are more suitable for further applications on advanced cutting edge research fields as mentioned above. Boron, which has only one p electron, is a neighboring element with carbon in the periodic table, thus it has been prompted that boron could also form nanostructures (or, in general, boron clusters). Boron atom also tends to form sp^2 hybridization, while its electron deficiency leads to very diverse bonding features in boron clusters,[8] therefore, boron nanostructures have been widely investigated. Since boron-based structures are not be found in nature, studies that includes these structures needs to be carried out via theoretical nanoscopic simulations. A wide range of boron nanostructures, such as quasi planar clusters,[9] nanosheets,[10,11] nanotubes,[6,7,11,12] or fullerenes,[13−15,15,17,16] have been explored and studied due to their suitability for new devices.[16−19] Among these new boron nanostructures, hollow fullerene B_{80} has attracted considerable interest due to the existence of a stable cage B_{80} with icosaedral symmetry (I_h).[13] Later, other alternative B_{80} geometries with tetrahedral symmetry (T_h) and core−shell structure have been proposed.[20,21] This T_h symmetry seems to be thermodynamically more stable. However, Sadrzadeh et al. found that T_h symmetry is obtained by slight distortion of I_h structure. In fact, I_h and T_h structures (and other one with C_1 symmetry) are close in energy and have almost identical structure.[14] Although B_{80} has not yet been manufactured, theoretical simulations point out to a large cohesive energy (~5.76 eV/atom), high deformation temperature and high formational stability.[13,14,22−24] Meanwhile, a large number of computational works on its electronic structure, stability and reactivity,[14,15,23,25,26] have been studied along with various applications, including hydrogen storage or CO_2 capture, have been published.[26−28,28,29] Despite all these theoretical simulations, fullerene B_{80} still has unexplored applications in a liquid media. For instance, the successful application of its analogue fullerene C_{60} requires a deep understanding on its behavior in the solution state, i.e., C_{60} needs to be solubilized.[30] As matter of fact, a huge effort to improve the poor solubility of C_{60} is being carried out.[30−32] To our knowledge, studies on the solvation of fullerene B_{80} has not been reported in the open literature up to date.

Among the plethora of solvents, ionic liquids (IL) have proven to be suitable alternatives to traditional solvents due to their unique features such as good thermal and chemical stability, non flammability and almost null vapor pressure.[32] Moreover, IL can be designed for task-specific applications by using the flexibility to alternate the ions combinations.[33−37] The analysis of the literature shows lack of data on fullerene B_{80} solvation, although ILs have been proposed as candidates for C_{60} solvation.[36−38] Previous studies were pointed out that the solvation shell around the C_{60} fullerene is mainly characterized

Received: May 31, 2015
Revised: August 3, 2015
Published: August 31, 2015

 © 2015 American Chemical Society

DOI: 10.1021/acs.jpcb.5b05187
J. Phys. Chem. B 2015, 119, 12455−12463

by ion-C_{60} $\pi-\pi$ stacking interactions. Yet, further analysis on the interaction mechanism between 24 IL and C_{60} through density functional theory simulations revealed that C_{60} solvation could be also achieved by ILs with deep HOMO energy level and week interionic interactions as well.[39] In this sense, Jang et al. studied C_{60} solvation by water molecules,[40] which revealed that negative fullerene surface potential along hydrogen bonding network around C_{60} is the main driving force for C_{60} self-aggregation in water.

At the molecular level, the solvation capability of ILs would be related with the strength of IL−B_{80} interactions, i.e. strengthening interaction energy is needed for stabilizing B_{80} fullerene in the solvent. Thus, interaction energy between B_{80} and ILs, estimated thorough DFT simulations, can be used as an approximation on inferring the main IL features at the molecular level needed for the design of task-specific ILs for B_{80} solvation. Hence, a DFT study on the interaction mechanism between selected ILs and fullerene B_{80} is reported in this work. Choline lactate ([CH][LAC]) and choline benzoate ([CH][BE]) ILs were selected in this work (Figure 1). Choline

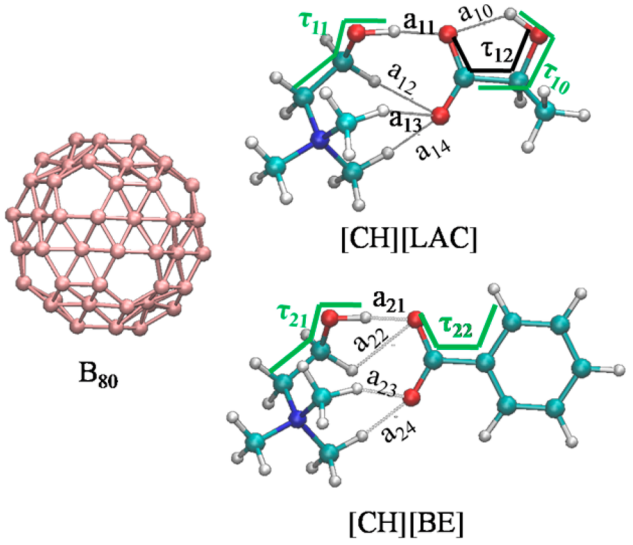

Figure 1. Optimized structure at PBE-D2/DZP level of buckyball B_{80} and [CH][LAC] and [CH][BE] ionic liquids. For ionic liquids, main structural parameters related with main intermolecular interactions are also labeled.

([CH]) cation-based ILs are a new generation of green solvents favorable properties such as null toxicity and high biodegradability.[41,42] Likewise, the combination of [CH] cation with lactate ([LA]) or benzoate ([BE]) anions can be recalled as biomaterials,[41] which can be produced at very considerably low cost[42] and near-zero environmental impact. As said, studies on the interaction between fullerene B_{80} and above-mentioned ILs (and in general any ionic liquid) are missing in literature; therefore this work provides in-depth information for the interaction mechanism between selected choline-based ionic liquids and B_{80}.

2. THEORETICAL DETAILS

DFT simulations were carried out using PBE functional[43] as implemented in the SIESTA 3.2 package,[44] along norm-conserving Troullier−Martins pseudopotentials[45] and numerical double-ζ polarized (DZP) basis sets. The PBE functional has been proven to perform well for large systems with a relatively low computational cost.[46−50] Ionic pair and IL−B_{80} interactions would involve a large component of noncovalent dispersion interactions. It is a well-known situation that dispersion interactions are not satisfactory described by ordinary DFT methods,[51] and thus, long-range dispersion corrections using the Grimme's scheme[52] were added to PBE functional (PBE-D2) and this method has been successfully applied to study pristine fullerene B_{80} and systems related to B_{80}.[12,21,24,29,53−56,53−56] All calculations were done with an energy mesh cutoff of 400 Ry, while structural relaxations were done by conjugate gradients, with convergence criteria enforced on all atoms which do not exceed 0.04 eV/Å.

Initial structure for B_{80} structure was obtained from the work of Muya et al.[24] and its optimization studies built on this extracted model. The optimized molecular structure in this work were compared with the structure reported by Muya et al.[24] and it is consistent with this previous study. [CH][LAC] and [CH][BE] ILs were previously studied by our group through DFT simulations[57,58] and their stable configurations were optimized at PBE-D2/DZP level. Once the B_{80} was fully optimized, one ionic pair was introduced to the simulations. In order to determine the most favorable position of the ionic pair, different structures were assessed as starting geometries (Figure S1, Supporting Information) for energy minimization. On the basis of the most favorable IL disposition onto the B_{80} surface, IL_n−B_{80} clusters composed by n ionic pairs (n = 2, 3, 4, 6) around one B_{80} were also optimized.

Atoms in molecules (AIM) theory[59] and the analysis of the reduced density gradient (RDG) at low densities[60] have been used for better understanding of the nature of the interaction mechanism. According to AIM theory, the existence of an interaction is indicated by the presence of a bond critical point (BCP), which can be featured based on its electronic density (ρ) and laplacian values ($\nabla^2\rho$). Similarly, ring/cage structures were characterized by their corresponding ring/cage critical point (RCP/CCP). Aimed at clarifying data analysis, attention has been mainly given on the bond critical points, while some information regarding to the adsorption process could also be obtained from ring and cage critical points. RDG analysis is based on electron density descriptor to identify the main interactions, which is based on the visualization of RDG isosurfaces. The isosurfaces of the reduced density gradient are defined as $s = (1/(2(3\pi^2)^{1/3}))((|\nabla\rho|)/(\rho^{1/3}))$; Strength and nature of the interactions is determined through the sign of the second density Hessian eigenvalue. Thus, by means of a color mapping scheme (based on the value of the electronic density times of the second eigenvalue of the Hessian), strong nonbonded overlaps appear as red regions, strong intermolecular interactions are plotted as a blue localized regions, while weak contacts (dispersive forces) appear as large green regions.[60] Charge transfer process were determined using the ChelpG method,[61] which has proven to be adequate for describing charge distributions in ILs.[57,62−65,62−65] AIM and RDG analysis were carried out using MultiWFN code,[66] which was also used to compute ChelpG atomic charges.

3. RESULTS AND DISCUSION

The study of IL−B_{80} systems is divided into three sections aimed at assessing the main features of the interaction between fullerene B_{80} and choline-based ILs. The first section analyzes the main properties related with the interaction between ions, which are need for a deeper understanding on the interaction mechanism between IL and B_{80}. The second section provides a

DOI: 10.1021/acs.jpcb.5b05187
J. Phys. Chem. B 2015, 119, 12455−12463

Table 1. Main Molecular Parameters of the Most Stable Optimized Structures of [CH][LAC] and [CH][BE] Ionic Liquids[a]

		[CH][LAC]				[CH][BE]		
		length/Å	ρ/au	$\nabla^2\rho$/au		length/Å	ρ/au	$\nabla^2\rho$/au
intermolecular interactions	a_{10} (O−H)	1.863	0.0360	0.1228				
	a_{11} (O−H)	1.512	0.0777	0.1122	a_{21} (O−H)	1.673	0.0668	0.1303
	a_{12} (O−H)	2.471	0.0111	0.0400	a_{22} (O−H)	1.980	0.0265	0.0843
	a_{13} (O−H)	2.029	0.0247	0.0777	a_{23} (O−H)	2.122	0.0213	0.0664
	a_{14} (O−H)	1.883	0.0309	0.1095	a_{24} (O−H)	1.816	0.0382	0.111 05
dihedral angles/degrees	τ_{10} (CCOH)	−1.0						
	τ_{11} (CCOH)	137.3			τ_{21} (CCOH)	132.3		
	τ_{12} (OCCO)	1.1			τ_{22} (OCCC)	0.0		
q^+ [b] /e^-		0.76				0.69		
BE_{IL} [c]/ kcal mol^{-1}		87.18 (4.59)				90.20 (4.60)		

[a]AIM parameters related with intermolecular interactions (electronic density, ρ, and its laplacian, $\nabla^2\rho$) as well as total charge over choline (q^+) and lactate or benzoate (q^-) ions computed according ChelpG scheme are also collected. See Figure 1 for labeling. [b]For isolated ionic liquids $q^+ = -q^-$. [c]Values in parentheses stand for dispersion contribution to the total binding.

detailed analysis of the interaction mechanism of IL−B_{80} systems. Therefore, properties such as binding energies, intermolecular interactions and electronic structure have been studied. The last section reports and insight into the first solvation shell of B_{80} by ILs. For this, DFT simulations of $(IL)_n$−B_{80} (n = 2, 3, 4, 6) have been also carried out.

3.1. [CH][LAC] and [CH][BE] Ionic Pairs. The main features of [CH][LAC] and [CH][BE] ILs have been previously studied by our group,[57,58] therefore in this work only the main features of these materials were analyzed and discussed. Figure 1 (*right*) shows optimized structures of the most stable conformations of both [CH][LAC] and [CH][BE] ILs at PBE-D2/DZP theoretical level, while Table 1 gathers the main parameter related with interactions between ions. Interionic binding energies (BE_{IL}) were used as a measurement of the interaction strength between ions and it is defined as

$$BE_{IL} = (E_{cat} + E_{ani}) - E_{IL} \quad (1)$$

where E_{cat}, E_{ani}, and E_{IL} stand for the total energy of the cation, anion, and ionic pair, respectively. Estimated BE_{IL} values are reported as 87.18 kcal mol^{-1} for [CH][LAC] and 90.20 kcal mol^{-1} for[CH][BE] (Table 1). Charge distributions were calculated according to the ChelpG model, and those results showed that the charge of ions is 0.76e^-/ 0.69e^-, in absolute value, for [CH][LAC]/[CH][BE] ILs, respectively, and thus showing an important charge transfer from the anion to the [CH] cation equivalent to 0.24 e^-/0.31 e^-, which is in agreement with the highest BE_{IL} value of [CH][BE] ionic liquid. Dispersion contributions (such as hydrogen bonds) also represent a small contribution to the total binding energy between ions. The optimized geometries show the presence of intermolecular hydrogen bonds between $[CH]^+$ cation and $[LAC]^-$ or $[BE]^-$ anions, through the cation hydroxyl and carboxylate groups in the corresponding ions (labeled as a_{11} or a_{21}, respectively). Likewise, an additional weak intermolecular hydrogen bond between COO^- group and H atoms in [CH] cation are also found (a_{11}−a_{14} and a_{21}−a_{24} for [CH][LAC] and [CH][BE] respectively). On the basis of shorter intermolecular bond length and AIM features (Table 1), intermolecular hydrogen bond between $[LAC]^-$ and $[CH]^+$ (a_{11} = 1.512, ρ = 0.0777 au) is slightly stronger than for $[BE]^-$ and $[CH]^+$ (a_{21} = 1.673, ρ = 0.0668 au). Nonetheless, the sum of the electronic density overall intermolecular interactions yields values slightly larger (0.0084 au) for [CH][BE. Table 1 also shows the dispersion energy contribution ($BE_{dis,IL}$) to the total binding energy values of around 4.60 kcal mol^{-1} for both ILs, which is quantified according to Grimme's approach for the PBE-D2 functional.[52]

3.2. IL−B_{80} Systems: Key Features of the Interaction Mechanism. Aimed at obtaining the most favorable disposition between selected ILs and fullerene B_{80}, different geometries were used as starting point for the optimizations (see Figure S1 and theoretical details in the Supporting Information). Among all essayed structures, those of minimal energy were further used for the analysis of IL−B_{80} systems. The most favorable configurations of ionic pairs interacting with B_{80} are reported in Figures 2 and 3, while the main parameters (intermolecular bond lengths and their AIM features, charge distributions, and binding energies) are collected in Table 2. The main features of ILs adsorbed on the surface of fullerene B_{80} is discussed herein. Several authors have pointed out that the change on cation−anion interaction strength can be used to understand the entropic contribution to

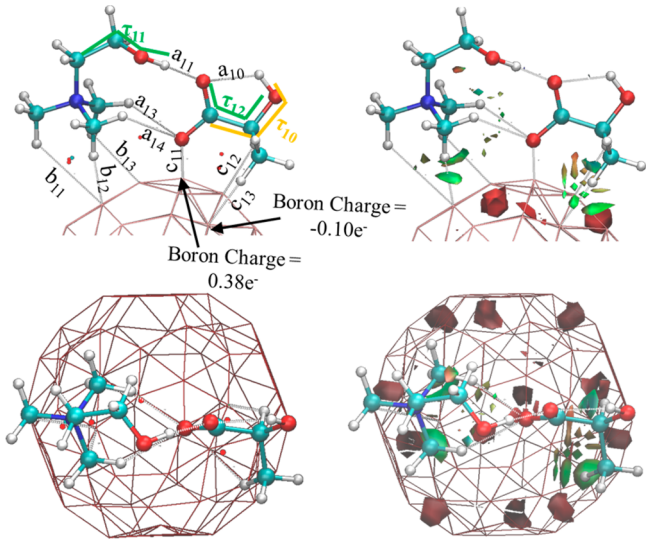

Figure 2. Side (up) and top (bottom) views for optimized structure at PBE-D2/DZP level corresponding to [CH][LAC]−B_{80} system along structural parameters related with intermolecular interactions (left) and RDG isosurfaces (right), whose green color indicates van der Waals interactions. Red and green points stand for RCP and CCP, respectively, related with intermolecular interactions. BCP were omitted for simplicity.

DOI: 10.1021/acs.jpcb.5b05187
J. Phys. Chem. B 2015, 119, 12455−12463

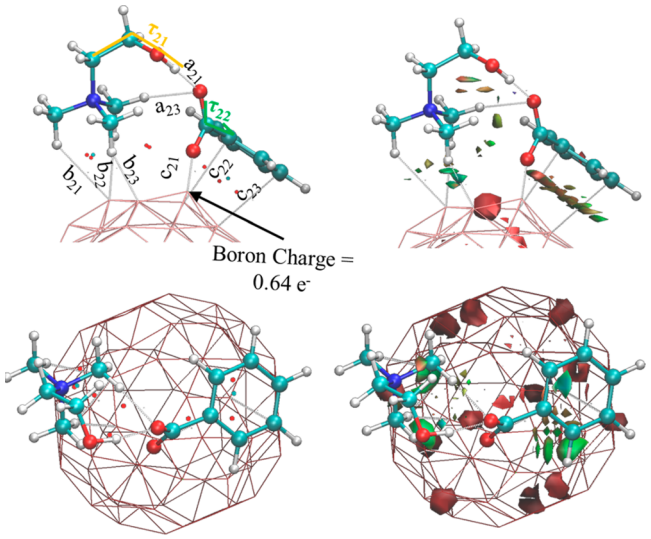

Figure 3. Side (up) and top (bottom) views for optimized structure at PBE-D2/DZP level corresponding to [CH][BE]−B_{80} system along structural parameters related with intermolecular interactions (left) and RDG isosurfaces (right), whose green color indicates van der Waals interactions. Red and purple points stand for RCP and CCP, respectively, related with intermolecular interactions. BCP were omitted for simplicity.

the solubility.[67,68] Therefore, the weakening of cation−anion interactions leads to an increase of free volume in the IL, which allows greater space to accommodate the solute molecules.[47]

Since coulomic forces stand for the main forces between ions in the ionic liquid bulk. BE_{IL} values have been calculated for both ILs but using their geometries taken from IL−B_{80} systems (Table 2). Both ILs diminish their binding energies up to 76.59 kcal mol^{-1} (energy diminution is equal to 10.59 kcal mol^{-1})/ 76.70 kcal mol^{-1} (13.50 kcal mol^{-1}) for [CH][LAC]/ [CH][BE]. For [CH][LAC] IL, the weakening in the interaction between ions is mainly due to two factors: (*i*) the small charge transfer from the surface anion to the surface of B_{80} (0.07 e^-) hinders the charge transfer process between ions, which is equal to 0.15 e^- (anion−cation charge transfer is equal to 0.24 e^- for the isolated ionic pair); (*ii*) softening of the intermolecular hydrogen bonds between ions (which can be assessed through the elongation of the intermolecular lengths as well as lower electronic density values), where even a_{12} was not found The main interaction between both ions (a_{11}) is elongated (0.161 Å) as well as its electronic density decreases, in agreement with a lower dispersion contribution (3.26 kcal mol^{-1} in comparison to 4.59 kcal mol^{-1} for isolated [CH][LAC]. Regarding the [CH][BE]−B_{80} system, the [BE] anion becomes slightly less negative, which allows a charge transfer to the B_{80} surface (0.07 e^-) while charge transfer (CT) between ions is not importantly affected (0.30 e^-). The presence of ullerene B_{80} carries the break of a_{22} and a_{23} intermolecular bond, while a_{21} and a_{23} slightly decrease (despite their bond lengths are shortened). As seen below, the largest charges on BE_{IL} values for [CH][BE] ionic liquids could be related to stronger IL−B_{80} interactions.

Table 2. Main Molecular Parameters for the Most Stable Structures Optimized at PBE-D2/DZP Levels of IL−B_{80} Systems[a]

[CH][LAC]				[CH][BE]			
	length/Å	ρ/au	$\nabla^2\rho$/au		length/Å	ρ/au	$\nabla^2\rho$/au
a_{10} (O−H)	1.995	0.0273	0.1070				
a_{11} (O−H)	1.673	0.0551	0.1419	a_{21} (O−H)	1.668	0.0500	0.1387
a_{13} (O−H)	2.381	0.0112	0.0391	a_{23} (O−H)	2.097	0.0198	0.0680
a_{14} (O−H)	2.777	0.0053	0.0208				
τ_{10} (CCOH)	8.5						
τ_{11} (CCOH)	−12.0			τ_{21} (CCOH)	−59.6		
τ_{12} (OCCO)	124.2			τ_{22} (OCCC)	103.8		
b_{11} (H−B)	2.604	0.0044	0.0110	b_{21} (H−B)	2.877	0.0072	0.0168
b_{12} (H−B)	2.442	0.0141	0.0276	b_{22} (H−B)	2.197	0.0209	0.0361
b_{13} (H−B)	2.427	0.0149	0.0380	b_{23} (H−B)	2.313	0.0167	0.0299
c_{11} (O−B)	1.501	0.1375	0.5388	c_{21} (O−B)	1.512	0.1351	0.5001
c_{12} (H−B)	2.396	0.0202	0.0359	c_{22} (H−B)	2.852	0.0157	0.0367
c_{13} (H−B)	2.599	0.0096	0.0323	c_{23} (H−B)	3.074	0.0112	0.0294
$\sum\rho_{(BCP,cat)}$[b]		0.0334		$\sum\rho_{(BCP,cat)}$[b]		0.0448	
$\sum\rho_{(BCP,ani)}$[b]		0.1673		$\sum\rho_{(BCP,ani)}$[b]		0.1620	
$\sum\rho_{(RCP)}$[c]		0.0351		$\sum\rho_{(RCP)}$[c]		0.0554	
$\sum\rho_{(CCP)}$[d]		0.0042		$\sum\rho_{(CCP)}$[d]		0.0106	
			$q^+/q^-/q^{B80}$/e$^-$				
	0.85/−0.78/−0.07				0.70/−0.63/−0.07		
			BE_{IL}[e]/ kcal mol^{-1}				
	76.59 (3.26)				76.70 (3.35)		
			$BE_{IL\text{-}B80}$[e]/kcal mol^{-1}				
	43.86 (16.22)				45.95 (22.04)		

[a]Binding energies, AIM parameters related with intermolecular interactions (electronic density, ρ, and its laplacian, $\nabla^2\rho$) as well as total charge over choline (q^+), lacate/benzoate (q^-) ions and B_{80} (q^{B80}) computed according to ChelpG scheme are also collected. See Figures 2 and 3 for labeling. [b]$\sum\rho_{(BCP)}$ represents the sum of ρ for those BCPs related with intermolecular interactions between the IL and B_{80}. [c]$\sum\rho_{(RCP)}$ represents the sum of ρ for those RCPs related with intermolecular interactions between the IL and B_{80}. [d]$\sum\rho_{(CCP)}$ represents the sum of ρ for those CCPs related with intermolecular interactions between the IL and B_{80}. [e]Values in parentheses stand for dispersion contribution to the total binding energy.

DOI: 10.1021/acs.jpcb.5b05187
J. Phys. Chem. B 2015, 119, 12455−12463

The strength of IL−B_{80} interactions is related with the suitability of ILs as B_{80} solvents. Binding energies of IL−B_{80} systems ($BE_{IL\text{-}B80}$) were defined as

$$BE_{IL-B80} = (E_{B80} + E_{IL}) - E_{IL-B80} \quad (2)$$

where E_{B80}, E_{IL}, and $E_{IL\text{-}B0}$ are the total energy of the fullerene, ionic pair, and IL−B_{80}, respectively. As seen in Table 2, binding energies lie between 43.86 kcal mol^{-1} for [CH][LAC] and 45.95 kcal $mol^{-1}$for [CH][BE], where dispersion contributions (36.98% and 47.97% for [CH][LAC] and [CH][BE] respectively) would be one of the main factors.

Interactions between [CH]-based ILs and fullerene B_{80} have been described through the topological analysis of the electronic density (AIM theory) and RDG isosurfaces, Figures 2 and 3. Green color of the regions between the IL and B_{80} molecule points out van der Waals interactions as the main driving force. Aimed at studying all BCPs as a whole, we have defined the sum of the electronic density ($\sum\rho_{(BCP)}$) over all BCPs related with cation/anion−B_{80} interactions: $\sum\rho_{(BCP)} = \sum\rho_{(BCP,cat)} + \sum\rho_{(BCP,ani)}$ (see Table 2). Instead of the selected IL, cation−B_{80} interactions take place through hydrogen bonds between H atoms of methyl groups and negatively charged boron atoms, with bond lengths equal to (in average) 2.491 Å/2.462 Å for [CH][LAC]/[CH][BE] ILs, while $\sum\rho_{(BCP,cat)}$= 0.0334 au/0.0448 au

The main feature of anion−B_{80} interactions is characterized by the presence of a chemical bond between COO^- group and B_{80} surface (c_{11}/c_{21} for [CH][LAC]/[CH][BE]). The laplacian of the electronic density ($\nabla^2\rho$) can be used to classify different bonds as $\nabla^2\rho > 0$ the bond is defined as closed-shell interaction (which could be an ionic, hydrogen or van der Waals bond); (ii) $\nabla^2\rho < 0$ the bond is defined as shared interaction (i.e., a covalent bond).[69] For both ionic liquids, O−B interaction between carboxilate moiety and B_{80} surface yields a $\nabla^2\rho$ values larger than zero. In addition, the absence of RDG isosurface between both O and B atoms as well as the (small) charge transfer from the anion to the B_{80} surface would point out to the presence of an ionic bond between the COO− moiety and the B_{80} surface. In addition, both bonds yield electronic density values of around 0.1363 au, which is in agreement with values obtained for other system with typical ionic bonds.[70]

Although both c_{11} and c_{21} bonds show similar features, there are differences in anion−B_{80} interactions. In addition to the O−B bond (c_{11}), [LA]−B_{80} interactions are set up between H atoms located in methyl groups (c_{12} and c_{13}) and the B_{80} surface, with a bond length of around 2.498 Å. Regarding to [BE]−B_{80} interactions, there is a clear π-stacking between phenyl moiety and the B_{80} surface, with a distance of around 3.0 Å. Palusiak et al.[71] found that ring critical point features (mainly the electronic density, ρ) are connected with the π-electronic delocalization. Then, we have conjectured a relationship of electronic delocalization between IL and B_{80} and $\sum\rho_{(RCP)}$. Although both ILs yield similar $\sum\rho_{(BCP,ani)}$ values, larger values of $\sum\rho_{(RCP)}$ for [CH][BE] IL agrees with a higher electronic delocalization due to the π-stacking as well as with a larger dispersion contribution to the total $BE_{IL\text{-}B80}$. Therefore, the greatest BE_{IL} diminution for [CH][BE] is related to stronger IL−B_{80} interactions.

For simplicity, discussions on the B_{80} structure were not deeply done herein as they have been extensively studied in the literature by itself.[14,15,23,25,26] The presence of a chemical bond between COO^- group and B_{80} leads to a small distortion of B_{80} symmetry, which has not dramatic effects on the features of fullerene B_{80}. For instance, as seen bellow, density of states of pristine B_{80} is very similar than partial density of states from B_{80} in IL−B_{80} systems. Another important feature is the atomic charge distribution of B_{80}. Published works assessing charge distribution of B_{80} are based on Mulliken atomic charges.[24,29] ChelpG charge distribution of pristine B_{80} leads to similar qualitative results, i.e. boron atoms in the center of hexagonal faces own positive charge, whereas frame boron atoms are negatively charged. The bond between COO^- group and boron surface is carried out with a positive charged boron atom located in the center of a hexagonal face (see Figures 2 and 3). Nonetheless, hydrogen bond labeled as c_{13} in [CH][LAC]−B_{80} system brings that a boron atom located in the center of a hexagonal face becomes negative charged. Although this is a very weak bond (see AIM features in Table 2), this new charge distribution could promote some B_{80} stability problems.

The results reported in this section confirm that [CH][LAC] and [CH][BE] ionic liquids would distort B_{80} geometry, which could be a problem for the use of B_{80} dispersed in ILs. The selection of these ILs were based on considering the absence of previous studies and targeted to minimize both the economic[42] and environmental isues[41] that are related with the use of classical ILs. Nevertheless, the results reported in this work reveal useful conclusions for the search of task-specific ILs regarding to B_{80} solvation. Ions with aromatic motifs could be adequate as B_{80} solvents due to strong interactions through $\pi-\pi$ stacking; whereas anions with functional groups, which tend to allocate much of its negative charge (e.g., COO^-), shall be avoided.

The main features of the electronic structure of IL−B_{80} systems were also studied. Figure S2 (Supporting Information) shows the total density of states (DOS) of pristine B_{80} and IL−B_{80} systems as well as the partial density of states (PDOS) corresponding to B_{80} contributions for IL−B_{80} systems. The total density of states of pristine B_{80} and the partial density of states corresponding to B_{80} atoms in IL−B_{80} systems own similar contours. Therefore, interactions with the selected ILs do not have large effects on the electronic structure of fullerene B_{80}. Figure 4 shows the partial density of states from both ions for isolated ILs and both IL−B_{80} systems as well as the molecular orbital contours for the highest occupied and lowest unoccupied molecule orbitals (HOMO and LUMO) of the ILs. For isolated [CH] and[LA]ILs, HOMO/LUMO levels are mainly delocalized over [LA] anion/[CH] cation, with a HOMO−LUMO energy gap $\Delta E_{H\text{-}G}$ = 3.96 eV. Regarding [CH][BE] IL, the HOMO orbital is mainly over carboxylate group with some contribution from the cation, while the LUMO level is mainly localized over the [BE] anion, where $\Delta E_{H\text{-}G}$ = 3.63 eV. Because of the interaction with B_{80}, LUMO orbital becomes LUMO+1, whose energy destabilization is equal to 0.37 eV/1.10 eV for [LA]/[BE] anions. Both HOMO and LUMO orbitals corresponding to the ionic liquid are delocalized over the anion, although they also own an important contribution from B_{80} fullerene, which agrees with the charge transfer process between the ionic liquid and B80 above-described. Both HOMO energies are of around −6.37 eV, while $\Delta E_{H\text{-}G}$ = 4.28 eV/3.70 eV for [CH][LAC]/[CH][BE], which is due to a deeper LUMO orbital over [BE] anion.

3.3. $(IL)_n$−B_{80} Systems: An Approach to the First Solvation Shell. Having discussed the features of the interaction mechanism between two [CH] based ILs and fullerene B_{80}, this section mainly pursues obtaining information

DOI: 10.1021/acs.jpcb.5b05187
J. Phys. Chem. B 2015, 119, 12455−12463

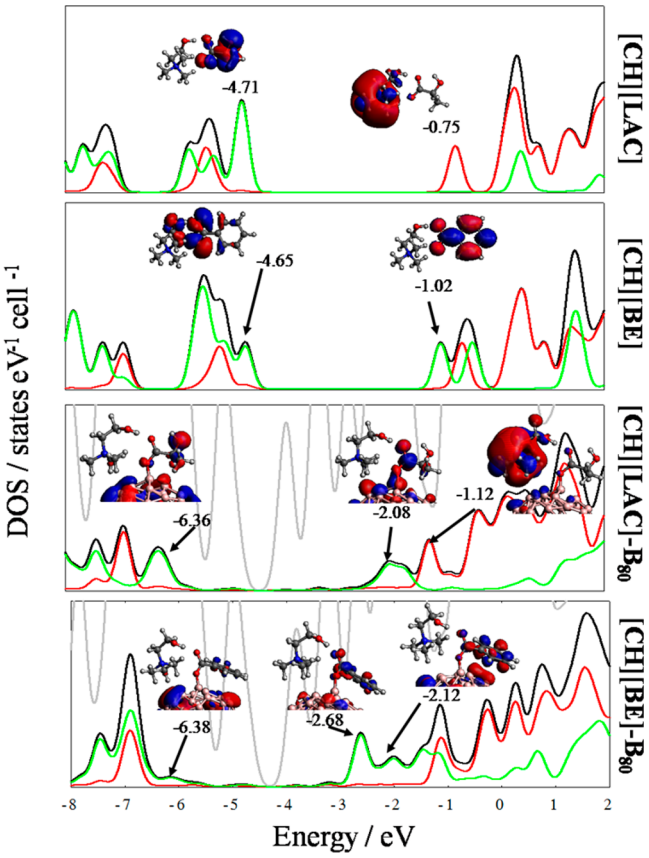

Figure 4. Density of states of both ionic pairs (black) and IL−B_{80} systems (gray), partial density of states of the cation (red) and anion (green). Molecular orbital contours corresponding to the highest/lowest occupied/unoccupied molecular orbitals located over ionic liquids along their energies are also indicated.

about the first IL solvation shell around of fullerene B_{80} through the study of system composed by one fullerene and a variable number of ionic pairs (n). On the basis of the most stable configuration above-described, $(IL)_n$−B_{80} systems (with n = 2, 3, 4 and 6) have been optimized. The binding energy as a function of n was calculated as follows:

$$BE_{(IL)n-B80} = [(E_{B80} + nE_{IL}) - E_{(IL)n-B80}] \quad (3)$$

where $E_{(IL)n-B0}$ is the total energy of $(IL)_n$−B_{80} system. The evolution of $BE_{(IL)n-B80}$ is shown in Figure 5. According to this

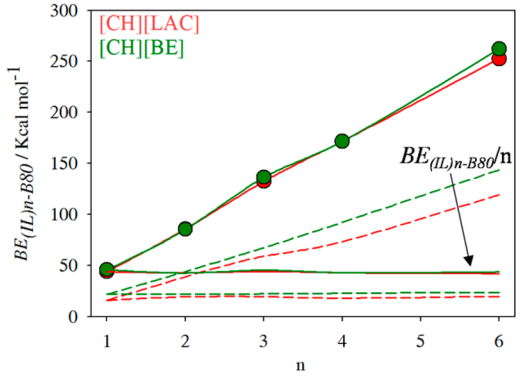

Figure 5. Binding energies of $(IL)_n$−B_{80}. Dotted lines represent the contribution from dispersion corrections.

figure $BE_{(IL)n-B80}$ increases as a function of n from 43.86 kcal mol^{-1}/45.95 kcal mol^{-1} (for [CH][LAC]/[CH][BE]) at n = 1 to 252.49 kcal mol^{-1}/262.16 kcal mol^{-1} at n = 6, with dispersion contributions lying between 16.22 kcal mol^{-1}/22.04 kcal mol^{-1} and 119.39 kcal mol^{-1}/143.75 kcal mol^{-1}. Figure 5 also draws $BE_{(IL)n-B80}$ per ionic pair ($BE_{(IL)n-B80}/n$), whose average values per ionic pair are 43.18 and 44.13 kcal mol^{-1} for [CH][LAC] and [CH][BE], respectively. These values per ionic pair are very close to that are computed for IL−B_{80} systems, which suggest that IL−B_{80} interactions is the main contribution to the total $BE_{(IL)n-B80}$. As expected, dispersion energy is one of the main contributions to the total energy, in average, dispersion contributions supply 43.34% and 51.45%to the total $BE_{(IL)n-B80}$ per ionic pair for [CH][LAC] and [CH][BE], respectively. For $(IL)_n$−B_{80} systems, this slightly increase in the dispersion contribution could be to ion−ion interactions between different ionic pairs. Figures 6 and 7

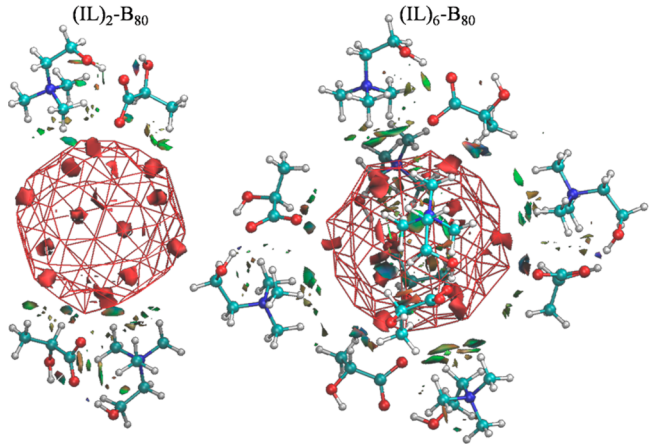

Figure 6. Optimized structures along to RDG isosurfaces of $([CH][LAC])_n$−B_{80} systems (n = 2,6).

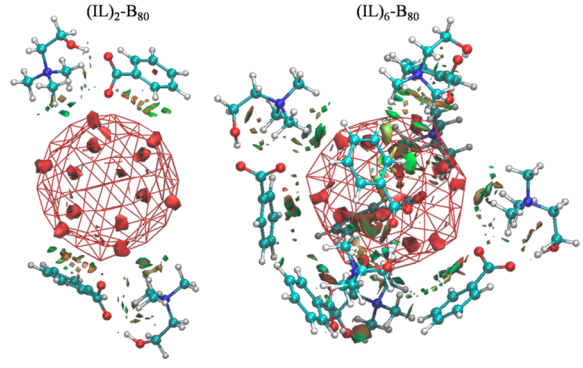

Figure 7. Optimized structures along to RDG isosurfaces of $([CH][BE])_n$−B_{80} systems (n = 2,6).

illustrate optimized structure of $(IL)_n$−B_{80} (n = 2, 6) along RDG isosurfaces. As previously noted, their green colors also suggest that dispersion interactions play one of the main roles in the interaction between ILs and B_{80}. Figure 8 plots the evolution of the total charge over the cation, the anion and B_{80} as a function of n. Although B_{80} gains a negative charge equal to 0.07 e^- for n = 1, it charge becomes to be ≃ 0.0 from $n \geq 3$. In the same way, a positive/negative charge over the cation/anion also shows an asymptotic behavior with n, with a charge of

DOI: 10.1021/acs.jpcb.5b05187
J. Phys. Chem. B 2015, 119, 12455−12463

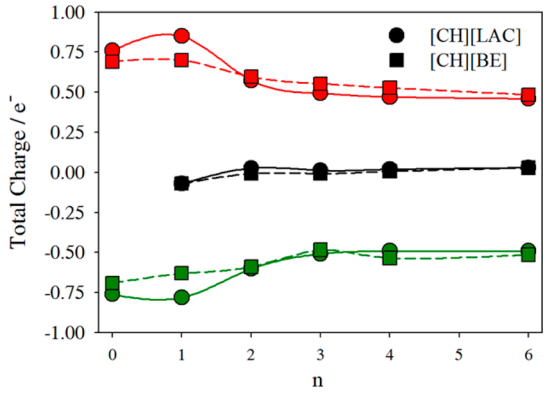

Figure 8. Evolution of the total charge over the cation (red), the anion (green), and B_{80} fullerene (black). Total charges over ions are average value per ion. Points at $n = 0$ stands for isolated ionic liquids.

around +0.50 e^-/−0.50 e^-. Thus, B_{80} could be able to disturb charge distribution in the IL bulk.

4. CONCLUSIONS

In this work, DFT simulations were performed to obtain insights on the interaction mechanism and the approximation to the solvation of fullerene B_{80} with ILs As a first approximation, solvation capability has been assessed through binding energies between selected ILs and B_{80} molecule for systems composed by one ionic pair and one fullerene B_{80}. Low toxic and biodegradable [CH] cation based ILs paired with [LAC] and [BE] anions were selected. DFT simulations results showed that a bond (which shows ionic character) is formed between COO^-group in the anion with one boron atom in the fullerene B_{80},which arises issues for the use of B_{80} dispersed in ILs. Nevertheless, our results also revealed useful information for the search of task-specific ILs for B_{80} solvation. It can be concluded that ions with aromatic motifs could be adequate as B_{80} solvents due to strong interactions through π-stacking.B_{80} atoms develop hydrogen bonding with nonaromatic [CH] cation, with boron atoms acting as hydrogen bond acceptors. Finally, information about the first solvation shell has been obtained through the optimization of $(IL)_n$−B_{80} systems with up to 6 ionic pair interacting with one fullerene B_{80}.

This work offers an insight up to the key parameters governing B_{80} solvation by ILs at the molecule level, providing some key ideas for the search of task specific solvent for B_{80}. Although the application of new system based on B_{80} systems is still an unexplored field, a deep understanding of its behavior in solution (for instance dispersed in ILs) can increase its potential applications.

■ ASSOCIATED CONTENT

Supporting Information

The Supporting Information is available free of charge on the ACS Publications website at DOI: 10.1021/acs.jpcb.5b05187.

Detailed description of the conformational search procedure with examples (Figure S1) and density of states of B_{80}, and IL−B_{80} systems (Figure S2) (PDF)

■ AUTHOR INFORMATION

Corresponding Authors

*E-mail: sapar@ubu.es. Telephone: +34 947 258 062 (S.A.).

*E-mail: mert.atilhan@qu.edu.qa. Telephone: +947 4403 4142 (M.A.).

Notes

The authors declare no competing financial interest.

■ ACKNOWLEDGMENTS

Gregorio García acknowledges the funding by Junta de Castilla y León (Spain), cofunded by European Social Fund, for a postdoctoral contract. This work was funded by Ministerio de Economía y Competitividad (Spain, project CTQ2013-40476-R) and Junta de Castilla y León (Spain, project BU324U14). We also acknowledge The Foundation of Supercomputing Center of Castile and León (FCSCL, Spain), Computing and Advanced Technologies Foundation of Extremadura (CénitS, LUSITANIA Supercomputer, Spain) and Consortium of Scientific and Academic Services of Cataluña (CSUC, Spain) for providing supercomputing facilities. This work was also made possible by NPRP grant # 6-330-2-140 from the Qatar National Research Fund (a member of Qatar Foundation). We also thank Dr. J. T. Muya and A. Ceulemans (University of Richmond) for providing us the optimized structures of pristine B_{80}. The statements made herein are solely the responsibility of the authors.

■ REFERENCES

(1) Wassei, J. K.; Kaner, R. B. Oh, the Places You'll Go with Graphene. *Acc. Chem. Res.* **2013**, *46*, 2244−2253.

(2) Hu, X.; Zhou, Q. Health and Ecosystem Risks of Graphene. *Chem. Rev.* **2013**, *113*, 3815−3835.

(3) Mao, H. Y.; Laurent, S.; Chen, W.; Akhavan, O.; Imani, M.; Ashkarran, A. A.; Mahmoudi, M. Graphene: Promises, Facts, Opportunities, and Challenges in Nanomedicine. *Chem. Rev.* **2013**, *113*, 3407−3424.

(4) Palermo, V. Not a Molecule, not a Polymer, not a Substrate··· the Many Faces of Graphene as a Chemical Platform. *Chem. Commun.* **2013**, *49*, 2848−2857.

(5) Karousis, N.; Tagmatarchis, N.; Tasis, D. Current Progress on the Chemical Modification of Carbon Nanotubes. *Chem. Rev.* **2010**, *110*, 5366−5397.

(6) Tang, H.; Ismail-Beigi, S. Novel Precursors for Boron Nanotubes: The Competition of Two-Center and Three-Center Bonding in Boron Sheets. *Phys. Rev. Lett.* **2007**, *99*, 115501.

(7) Yang, X.; Ding, Y.; Ni, J. Ab Initio Prediction of Stable Boron Sheets and Boron Nanotubes: Structure, Stability, and Electronic Properties. *Phys. Rev. B: Condens. Matter Mater. Phys.* **2008**, *77*, 041402.

(8) Yan, Q. B.; Sheng, X. L.; Zheng, Q. R.; Zhang, L. Z.; Su, G. Family of Boron Fullerenes: General constructing Schemes, Electron Counting Rule, and Ab Initio Calculations. *Phys. Rev. B: Condens. Matter Mater. Phys.* **2008**, *78*, 201401.

(9) Boustani, I. Systematic Ab Initio Investigation of Bare Boron Clusters: Determination of the Geometry and Electronic Structures of Bn (n = 2−14). *Phys. Rev. B: Condens. Matter Mater. Phys.* **1997**, *55*, 16426−16438.

(10) Lau, K. C.; Pandey, R. Stability and Electronic Properties of Atomistically-Engineered 2D Boron Sheets. *J. Phys. Chem. C* **2007**, *111*, 2906−2912.

(11) Lau, K. C.; Pati, R.; Pandey, R.; Pineda, A. C. First-Principles Study of the Stability and Electronic Properties of Sheets and Nanotubes of Elemental Boron. *Chem. Phys. Lett.* **2006**, *418*, 549−554.

(12) Singh, A. K.; Sadrzadeh, A.; Yakobson, B. I. Probing Properties of Boron α-Tubes by Ab Initio Calculations. *Nano Lett.* **2008**, *8*, 1314−1317.

(13) Gonzalez Szwacki, N.; Sadrzadeh, A.; Yakobson, B. I. B80 Fullerene: An Ab Initio Prediction of Geometry, Stability, and Electronic Structure. *Phys. Rev. Lett.* **2007**, *98*, 166804.

DOI: 10.1021/acs.jpcb.5b05187
J. Phys. Chem. B 2015, 119, 12455−12463

(14) Sadrzadeh, A.; Pupysheva, O. V.; Singh, A. K.; Yakobson, B. I. The Boron Buckyball and Its Precursors: An Electronic Structure Study. *J. Phys. Chem. A* **2008**, *112*, 13679−13683.
(15) Muya, J. T.; De Proft, F.; Geerlings, P.; Nguyen, M. T.; Ceulemans, A. Theoretical Study on the Regioselectivity of the B80 Buckyball in Electrophilic and Nucleophilic Reactions Using DFT-Based Reactivity Indices. *J. Phys. Chem. A* **2011**, *115*, 9069−9080.
(16) Zheng, X. H.; Hao, H.; Lan, J.; Wang, X. L.; Shi, X. Q.; Zeng, Z. First Principles Study on the Electronic Transport Properties of C60 and B80 Molecular Bridges. *J. Appl. Phys.* **2014**, *116*, 073703.
(17) Yun, S. H.; Wu, J. Z.; Dibos, A.; Zou, X.; Karlsson, U. O. Self-Assembled Boron Nanowire Y-Junctions. *Nano Lett.* **2006**, *6*, 385−389.
(18) Sivaev, I. B.; Bregadze, V. V. Polyhedral Boranes for Medical Applications: Current Status and Perspectives. *Eur. J. Inorg. Chem.* **2009**, *2009*, 1433−1450.
(19) He, H.; Pandey, R.; Boustani, I.; Karna, S. P. Metal-like Electrical Conductance in Boron Fullerenes. *J. Phys. Chem. C* **2010**, *114*, 4149−4152.
(20) Li, H.; Shao, N.; Shang, B.; Yuan, L.-F.; Yang, J.; Zeng, X. C. Icosahedral B12-Containing Core-Shell Structures of B80. *Chem. Commun.* **2010**, *46*, 3878−3880.
(21) Zhao, J.; Wang, L.; Li, F.; Chen, Z. B80 and Other Medium-Sized Boron Clusters: Core−Shell Structures, Not Hollow Cages. *J. Phys. Chem. A* **2010**, *114*, 9969−9972.
(22) Gonzalez Szwacki, N.; Sadrzadeh, A.; Yakobson, B. I. Erratum: B80 Fullerene: An Ab Initio Prediction of Geometry, Stability, and Electronic Structure [Phys. Rev. Lett. 98, 166804]. *Phys. Rev. Lett.* **2008**, *100*, 159901.
(23) Hayami, W.; Otani, S. Structural Stability of Boron Clusters with Octahedral and Tetrahedral Symmetries. *J. Phys. Chem. A* **2011**, *115*, 8204−8207.
(24) Muya, J. T.; Lijnen, E.; Nguyen, M. T.; Ceulemans, A. The Boron Conundrum: Which Principles Underlie the Formation of Large Hollow Boron Cages? *ChemPhysChem* **2013**, *14*, 346−363.
(25) Ceulemans, A.; Muya, J. T.; Gopakumar, G.; Nguyen, M. T. Chemical Bonding in the Boron Buckyball. *Chem. Phys. Lett.* **2008**, *461*, 226−228.
(26) Bean, D. E.; Muya, J. T.; Fowler, P. W.; Nguyen, M. T.; Ceulemans, A. Ring Currents in Boron and Carbon Buckyballs, B80 and C60. *Phys. Chem. Chem. Phys.* **2011**, *13*, 20855−20862.
(27) Li, M.; Li, Y.; Zhou, Z.; Shen, P.; Chen, Z. Ca-Coated Boron Fullerenes and Nanotubes as Superior Hydrogen Storage Materials. *Nano Lett.* **2009**, *9*, 1944−1948.
(28) Wu, G.; Wang, J.; Zhang, X.; Zhu, L. Hydrogen Storage on Metal-Coated B80 Buckyballs with Density Functional Theory. *J. Phys. Chem. C* **2009**, *113*, 7052−7057.
(29) Sun, Q.; Wang, M.; Li, Z.; Du, A.; Searles, D. J. Carbon Dioxide Capture and Gas Separation on B80 Fullerene. *J. Phys. Chem. C* **2014**, *118*, 2170−2177.
(30) McHedlov-Petrossyan, N. O. Fullerenes in Liquid Media: An Unsettling Intrusion into the Solution Chemistry. *Chem. Rev.* **2013**, *113*, 5149−5193.
(31) Wang, C. I.; Hua, C. C.; Chen, S. A. Dynamic Solvation Shell and Solubility of C60 in Organic Solvents. *J. Phys. Chem. B* **2014**, *118*, 9964−9973.
(32) Earle-Martyn, J.; Seddon-Kenneth, R. Ionic Liquids: Green Solvents for the Future. In *Clean Solvents*; American Chemical Society: Washington, DC, 2002.
(33) Wilkes, J. S. A Short History of Ionic Liquids-from Molten Salts to Neoteric Solvents. *Green Chem.* **2002**, *4*, 73−80.
(34) Rogers, R. D.; Seddon, K. R. Ionic Liquids–Solvents of the Future? *Science* **2003**, *302*, 792−793.
(35) Lei, Z.; Dai, C.; Chen, B. Gas Solubility in Ionic Liquids. *Chem. Rev.* **2014**, *114*, 1289−1326.
(36) Maciel, C.; Fileti, E. E. Molecular Interactions between Fullerene C60 and Ionic Liquids. *Chem. Phys. Lett.* **2013**, *568*−*569*, 75−79.
(37) García, G.; Atilhan, M.; Aparicio, S. Theoretical Study on the Solvation of C60 Fullerene by Ionic Liquids. *J. Phys. Chem. B* **2014**, *118*, 11330−11340.
(38) Chaban, V.; Maciel, C.; Fileti, E. Does the Like Dissolves Like Rule Hold for Fullerene and Ionic Liquids? *J. Solution Chem.* **2014**, *43*, 1019−1031.
(39) García, G.; Atilhan, M.; Aparicio, S. Theoretical Study on the Solvation of Fullerene C60 by Ionic Liquids. *J. Phys. Chem. B* **2015**, *119*, 10616.
(40) Choi, J. I.; Snow, S. D.; Kim, J.-H.; Jang, S. S. Interaction of C60 with Water: First-Principles Modeling and Environmental Implications. *Environ. Sci. Technol.* **2015**, *49*, 1529−1536.
(41) Petkovic, M.; Ferguson, J. L.; Gunaratne, H. Q. N.; Ferreira, R.; Leitao, M. C.; Seddon, K. R.; Rebelo, L. P. N.; Pereira, C. S. Novel Biocompatible Cholinium-Based Ionic Liquids-Toxicity and Biodegradability. *Green Chem.* **2010**, *12*, 643−649.
(42) Yu, Y.; Lu, X.; Zhou, Q.; Dong, K.; Yao, H.; Zhang, S. Biodegradable Naphthenic Acid Ionic Liquids: Synthesis, Characterization, and Quantitative Structure−Biodegradation Relationship. *Chem. - Eur. J.* **2008**, *14*, 11174−11182.
(43) Perdew, J. P.; Ernzerhof, K. B. Generalized Gradient Approximation Made Simple. *Phys. Rev. Lett.* **1996**, *77*, 3865.
(44) Soler, J. M.; Artacho, E.; Gale, J. D.; García, A.; Junquera, J.; Ordejón, P.; Sánchez-Portal, S. The SIESTA method for ab initio order-N materials simulation. *J. Phys.: Condens. Matter* **2002**, *14*, 2745.
(45) Troullier, N.; Martins, J. L. Efficient Pseudopotentials for Plane-Wave Calculations. *Phys. Rev. B: Condens. Matter Mater. Phys.* **1991**, *43*, 1993−2006.
(46) Hu, T.; Gerber, I. C. Theoretical Study of the Interaction of Electron Donor and Acceptor Molecules with Graphene. *J. Phys. Chem. C* **2013**, *117*, 2411−2420.
(47) Lechner, C.; Sax, A. F. Adhesive Forces Between Aromatic Molecules and Graphene. *J. Phys. Chem. C* **2014**, *118*, 20970−20981.
(48) Hummer, K.; Puschnig, P.; Ambrosch-Draxl, C. Ab Initio Study of Anthracene under High Pressure. *Phys. Rev. B: Condens. Matter Mater. Phys.* **2003**, *67*, 184105.
(49) Freitas, R. R. Q.; Rivelino, R.; Mota, F. d. B.; de Castilho, C. M. C. DFT Studies of the Interactions of a Graphene Layer with Small Water Aggregates. *J. Phys. Chem. A* **2011**, *115*, 12348−12356.
(50) Shayeganfar, F.; Rochefort, A. Electronic Properties of Self-Assembled Trimesic Acid Monolayer on Graphene. *Langmuir* **2014**, *30*, 9707−9716.
(51) Cohen, A. J.; Mori-Sánchez, P.; Yang, W. Challenges for Density Functional Theory. *Chem. Rev.* **2012**, *112*, 289−320.
(52) Grimme, S. Semiempirical GGA-Type Density Functional Constructed with a Long-Range Dispersion Correction. *J. Comput. Chem.* **2006**, *27*, 1787−1799.
(53) Mahdavifar, Z.; Poulad, M. Theoretical Prediction of Ozone Sensing using Pristine and Endohedral Metalloboron B80 Fullerenes. *Sens. Actuators, B* **2014**, *205*, 26−38.
(54) Sun, Q.; Wang, M.; Li, Z.; Du, A.; Searles, D. J. A Computational Study of Carbon Dioxide Adsorption on Solid Boron. *Phys. Chem. Chem. Phys.* **2014**, *16*, 12695−12702.
(55) Muya, J. T.; Ramanantoanina, H.; Daul, C.; Nguyen, M. T.; Gopakumar, G.; Ceulemans, A. Jahn-Teller Instability in Cationic Boron and Carbon Buckyballs B80+ and C60+: a Comparative Study. *Phys. Chem. Chem. Phys.* **2013**, *15*, 2829−2835.
(56) Sun, Q.; Wang, M.; Li, Z.; Ma, Y.; Du, A. CO2 Capture and Gas Separation on Boron Carbon Nanotubes. *Chem. Phys. Lett.* **2013**, *575*, 59−66.
(57) Aparicio, S.; Atilhan, M. A Computational Study on Choline Benzoate and Choline Salicylate Ionic Liquids in the Pure State and After CO2 Adsorption. *J. Phys. Chem. B* **2012**, *116*, 9171−9185.
(58) García, G.; Atilhan, M.; Aparicio, S. Water Effect on Acid-Gas Capture Using Choline Lactate: A DFT Insight beyond Molecule−Molecule Pair Simulations. *J. Phys. Chem. B* **2015**, *119*, 5546−5557.
(59) Bader, R. F. W. *Atoms in Molecules: a Quantum Theory*; Oxford: Oxford, U.K., 1990.

DOI: 10.1021/acs.jpcb.5b05187
J. Phys. Chem. B 2015, 119, 12455−12463

(60) Johnson, E. R.; Keinan, S.; Mori-Sánchez, P.; Contreras-García, J.; Cohen, A. J.; Yang, W. Revealing Noncovalent Interactions. *J. Am. Chem. Soc.* **2010**, *132*, 6498−6506.
(61) Breneman, C. M.; Wiberg, K. B. Determining Atom-Centered Monopoles from Molecular Electrostatic Potentials. The Need for High Sampling Density in Formamide Conformational Analysis. *J. Comput. Chem.* **1990**, *11*, 361−373.
(62) Aparicio, S.; Atilhan, M. Water effect on CO2 absorption for hydroxylammonium based ionic liquids: A molecular dynamics study. *Chem. Phys.* **2012**, *400*, 118−125.
(63) Aparicio, S.; Atilhan, M. Nanoscopic Vision on Fuel Dearomatization Using Ionic Liquids: The Case of Piperazine-Based Fluids. *Energy Fuels* **2013**, *27*, 2515−2527.
(64) Sanz, V.; Alcalde, R.; Atilhan, M.; Aparicio, S. Insights from Quantum Chemistry into Piperazine-Based Ionic Liquids and their behavior with regard to CO2. *J. Mol. Model.* **2014**, *20*, 1−14.
(65) Aparicio, S.; Atilhan, M. Computational Study of Hexamethylguanidinium Lactate Ionic Liquid: A Candidate for Natural Gas Sweetening. *Energy Fuels* **2010**, *24*, 4989−5001.
(66) Lu, T.; Chen, F. Multiwfn: A Multifunctional Wavefunction Analyzer. *J. Comput. Chem.* **2012**, *33*, 580−592.
(67) Damas, G. B.; Dias, A. B. A.; Costa, L. T. A Quantum Chemistry Study for Ionic Liquids Applied to Gas Capture and Separation. *J. Phys. Chem. B* **2014**, *118*, 9046−9064.
(68) Fernandes, A. M.; Rocha, M. A. A.; Freire, M. G.; Marrucho, I. M.; Coutinho, J. A. P.; Santos, L. M. N. B. F. Evaluation of Cation−Anion Interaction Strength in Ionic Liquids. *J. Phys. Chem. B* **2011**, *115*, 4033−4041.
(69) Popelier, P. L. A. Quantum Molecular Similarity. 1. BCP Space. *J. Phys. Chem. A* **1999**, *103*, 2883−2890.
(70) Gillespie, R. J. Electron Densities, Atomic Charges, and Ionic, Covalent, and Polar Bonds. *J. Chem. Educ.* **2001**, *78*, 1688.
(71) Palusiak, M.; Krygowski, T. M. Application of AIM Parameters at Ring Critical Points for Estimation of π-Electron Delocalization in Six-Membered Aromatic and Quasi-Aromatic Rings. *Chem. - Eur. J.* **2007**, *13*, 7996−8006.

DOI: 10.1021/acs.jpcb.5b05187
J. Phys. Chem. B 2015, 119, 12455−12463